Atmos. Chem. Phys., 12, 7753–7765, 2012
www.atmos-chem-phys.net/12/7753/2012/
doi:10.5194/acp-12-7753-2012

Atmospheric Chemistry and Physics

Observations of middle atmospheric H_2O and O_3 during the 2010 major sudden stratospheric warming by a network of microwave radiometers

D. Scheiben[1], C. Straub[1], K. Hocke[1,2], P. Forkman[3], and N. Kämpfer[1,2]

[1]Institute of Applied Physics, University of Bern, 3012 Bern, Switzerland
[2]Oeschger Center for Climate Change Research, University of Bern, 3012 Bern, Switzerland
[3]Department of Earth and Space Sciences, Chalmers University of Technology, Gothenburg, Sweden

Correspondence to: D. Scheiben (dominik.scheiben@iap.unibe.ch)

Received: 7 October 2011 – Published in Atmos. Chem. Phys. Discuss.: 8 December 2011
Revised: 17 August 2012 – Accepted: 17 August 2012 – Published: 28 August 2012

Abstract. In this study, we present middle atmospheric water vapor (H_2O) and ozone (O_3) measurements obtained by ground-based microwave radiometers at three European locations in Bern (47° N), Onsala (57° N) and Sodankylä (67° N) during Northern winter 2009/2010. In January 2010, a major sudden stratospheric warming (SSW) occurred in the Northern Hemisphere whose signatures are evident in the ground-based observations of H_2O and O_3. The observed anomalies in H_2O and O_3 are mostly explained by the relative location of the polar vortex with respect to the measurement locations. The SSW started on 26 January 2010 and was most pronounced by the end of January. The zonal mean temperature in the middle stratosphere (10 hPa) increased by approximately 25 Kelvin within a few days. The stratospheric vortex weakened during the SSW and shifted towards Europe. In the mesosphere, the vortex broke down, which lead to large scale mixing of polar and midlatitudinal air. After the warming, the polar vortex in the stratosphere split into two weaker vortices and in the mesosphere, a new, pole-centered vortex formed with maximum wind speed of $70\,\mathrm{m\,s^{-1}}$ at approximately 40° N. The shift of the stratospheric vortex towards Europe was observed in Bern as an increase in stratospheric H_2O and a decrease in O_3. The breakdown of the mesospheric vortex during the SSW was observed at Onsala and Sodankylä as a sudden increase in mesospheric H_2O. The following large-scale descent inside the newly formed mesospheric vortex was well captured by the H_2O observations in Sodankylä. In order to combine the H_2O observations from the three different locations, we applied the trajectory mapping technique on our H_2O observations to derive synoptic scale maps of the H_2O distribution. Based on our observations and the 3-D wind field, this method allows determining the approximate development of the stratospheric and mesospheric polar vortex and demonstrates the potential of a network of ground-based instruments.

1 Introduction

The lack of solar radiative heating at the pole leads to a large low pressure system during winter time. This low pressure system leads to strong eastward winds around the North Pole, forming the winter polar vortex. The edge of the vortex acts as a mixing barrier such that the air inside the vortex has a different chemical composition than outside (Schoeberl et al., 1992; Manney et al., 1994). The polar vortex exists from the lower stratosphere up to the mesosphere, but is strongest near the stratopause. In the mesosphere, the vortex area is usually larger than in the stratosphere, i.e. the polar night jet is located at lower latitudes than in the stratosphere (Harvey et al., 2009 and references therein). Inside the polar vortex, the air descends from the mesosphere to the stratosphere. This was modeled by e.g. Fisher et al. (1993) or observed by e.g. Allen et al. (2000). During a calm winter, the vortex persists until the beginning of spring. During some winters however, the polar vortex is seriously disturbed or even breaks down due to sudden stratospheric warmings (SSW), which were first observed by Scherhag (1952).

A SSW is a sudden increase in the stratospheric temperature, accompanied by a deceleration of the zonal mean eastward wind. The terms minor and major warming refer to the characterization of SSWs according to the Commission for Atmospheric Sciences of the World Meteorological Organization (WMO) and is based on the work of McInturff (1978). A SSW is called major if the zonal mean temperature on 10 hPa increases from 60° latitude towards the pole and if the zonal mean zonal wind on 10 hPa reverses poleward of 60° latitude. A major warming in the stratosphere is often accompanied by a cooling in the mesosphere that usually starts a few days earlier than the stratospheric warming (Schoeberl, 1978). The occurrence of SSWs is due to the interaction of westward propagating planetary waves with the zonal mean flow (eastward) (Matsuno, 1971). The breaking of these planetary waves acts to decelerate the zonal mean flow that leads to distortion and/or breakdown of the polar night jet. This wave-mean flow interaction triggers a displacement, disruption and/or splitting of the polar vortex (Charlton and Polvani, 2007). The strongest major SSW observed up to date occurred in late January 2009 (Manney et al., 2009; Labitzke and Kunze, 2009).

The coupling between two or more atmospheric layers during a SSW was the focus of many recent studies. Martius et al. (2009, and references therein) showed that tropospheric blocking situations could be a trigger of a SSW. Flury et al. (2009) showed that the major SSW during winter 2007/2008 was accompanied by a decrease in lower stratospheric ozone due to the formation of polar stratospheric clouds. At the same time, ozone decreased in the relatively warm upper stratosphere due to the temperature dependence of the NO_x cycle, which was modeled in their study. The effects of SSWs can extend to the subtropics, as was shown by De Wachter et al. (2011). During the SSW of 2008 they observed a decrease in mesospheric water vapor over Seoul, South Korea, that was attributed to advection of dry polar mesospheric air to the subtropics. Middle atmospheric water vapor was also used as tracer for calculating the descent rate of polar mesospheric air during winter (e.g. Siskind et al., 2007; Orsolini et al., 2010; Lahoz et al., 2011; Straub et al., 2012). Manney et al. (2008a and 2008b) and Orsolini et al. (2010) showed that after the major SSWs of 2004, 2006 and 2009, the stratopause and the eastward wind jet reformed at approximately 75 km altitude. Goncharenko et al. (2010) showed that SSWs also have an impact on winds, tides and composition of the lower thermosphere and ionosphere in the equatorial region.

In winter 2009/2010, two SSWs occurred in the Northern Hemisphere, a minor warming in early December 2009 and a major warming in late January 2010. In this study, we investigate the effects of the major SSW on H_2O and O_3 observations from ground-based microwave radiometers within the Network for the Detection of Atmospheric Composition Change (NDACC) across Europe from midlatitudes up to high latitudes. There is one midlatitude location, Bern, Switzerland (46.9° N/7.45° E) and two high latitude sites, Onsala, Sweden (57.4° N/12.0° E) and Sodankylä, Finland (67.4° N/26.6° E). We investigate the potential of such a mini-network to derive synoptical maps of the observed trace species by a domain-filling technique to determine the dynamical processes in the middle atmosphere during a SSW. Particularly the lifetime of H_2O below 70 km is long enough to apply domain-filling techniques. The examination of the potential of ground-based instruments is particularly important under the light of current satellite missions that phase out in the near future without successor missions (e.g. NASA's Aura satellite) or already phased out missions (e.g. ESA's Envisat).

Section 2 describes the data sources and methods and gives references for further details on the instruments. Section 3 gives a description of the major SSW in January 2010 in terms of the temporal evolution of the polar vortex during the SSW. A special analysis technique determines the vortex edge even in the mesosphere. In Sect. 4, we present the ground-based observations at the three sites and in Sect. 5, the H_2O observations are combined by trajectory mapping to yield a synoptical map of the H_2O distribution during the SSW. Section 6 summarizes the presented study.

2 Data and methods

2.1 Data sources

The data of the ground-based microwave radiometers are in the center of our study. In addition, data of a spaceborne microwave radiometer are used for comparison with the results of the ground-based network and with the definition of the vortex edge. Microwave radiometers are passive instruments measuring a pressure broadened rotational emission line of the molecule of interest, in the case of our ground-based radiometers 22 GHz for water vapor and 142 GHz for ozone. Pressure broadening allows retrieving a vertical profile of the molecule of interest for example by means of radiative transfer calculations and the Optimal Estimation Method (e.g. Rodgers, 2000). The upper limit of the retrieval is mainly determined by the resolution of the spectrometer, the lower limit by the total measured bandwidth and the baseline of the spectrum.

For Bern, Switzerland, H_2O profiles are retrieved from the H_2O line spectra of the MIddle Atmospheric WAter vapor RAdiometer (MIAWARA) at pressure levels from 10 to 0.02 hPa (Deuber et al., 2005). The temporal resolution depends on tropospheric opacity and is a few hours during wintertime. The vertical resolution ranges from 11 km in the stratosphere to 14 km in the mesosphere, the precision (1-sigma random uncertainty) from approximately 5 % in the stratosphere to 20 % in the mesosphere. MIAWARA was intercompared with other ground-based microwave radiometers and satellites yielding a bias of less than 10 percent in the stratosphere and mesosphere (Haefele et al., 2009). Ozone profiles for Bern are measured by the GROund-based Millimeter-wave Ozone Spectrometer (GROMOS), which has a valid vertical range between 60 and 0.1 hPa with a temporal resolution of a few minutes (Calisesi et al., 2001). The vertical resolution of GROMOS is approximately 10 km in the stratosphere and 20 km in the lower mesosphere and the precision ranges from 6 % in the stratosphere to 12 % in the mesosphere. In the present study, 2-hourly ozone retrievals are averaged to daily profiles. Both instruments, MIAWARA and GROMOS, are part of NDACC. NDACC instruments undergo a strict quality control and continuously provide measurements to the NDACC data center. The H_2O data presented for Onsala, Sweden, are also obtained by a ground-based microwave radiometer with similar characteristics as MIAWARA (Forkman et al., 2003) and is also part of NDACC. The valid vertical range of the Onsala H_2O radiometer is 4 to 0.02 hPa. There have been difficulties in the operation of this radiometer in winter 2009/2010 resulting in data gaps. The H_2O data over Sodankylä are obtained from the compact radiometer MIAWARA-C (Straub et al., 2010). This instrument, which has been specifically designed for the use in measurement campaigns, was operated at Sodankylä in the frame of the Lapland Atmosphere-Biosphere Facility (LAPBIAT) campaign. MIAWARA-C's daily profiles cover an altitude range between 10 and 0.02 hPa with a vertical resolution of approximately 12 km. The precision of MIAWARA-C ranges from 5 % in the stratosphere to 18 % in the mesosphere.

The Microwave Limb Sounder on NASA's Aura satellite (Aura MLS) is a passive limb sounder for the retrieval of various trace species, geopotential height and temperature data (Waters et al., 2006). The Aura MLS retrieval version used for this study is 3.3. The following numbers on spectral lines, vertical resolution and pressure range originate from the Aura MLS data quality documents on http://mls.jpl.nasa.gov/data/datadocs.php). The H_2O retrieval uses the spectral line at 183 GHz, the temperature retrieval at 118 and 240 GHz, the CO retrieval at 240 GHz and the N_2O retrieval at 640 GHz. The vertical resolution of Aura MLS H_2O ranges from 3 km in the stratosphere to approximately 10 km in the upper mesosphere. The vertical resolution of the temperature retrieval is approximately 4 km in the stratosphere and increases to 6 km in the upper mesosphere. For CO, the vertical resolution is in the range of 3.5 to 5 km from the upper troposphere to the lower mesosphere and degrades to approximately 7 km in the upper mesosphere. The N_2O vertical resolution is between 4 and 7 km. Data are only considered within the valid vertical range (316–0.002 hPa for H_2O, 261–0.001 hPa for temperature, 100–0.0046 hPa for CO and 100–0.46 hPa for N_2O) and if quality thresholds are met as given in the data quality documents of Aura MLS.

We use the operational analysis from the European Center for Medium-Range Weather Forecasts (ECMWF, http://www.ecmwf.int/products/data/operational_system/) for descriptions of the polar vortex and the trajectory calculations. The ECMWF model cycle used in this study is 36r1 (T1279) and has 91 vertical levels from the surface up to 0.01 hPa. The model data are retrieved on a regular latitude/longitude grid at a resolution of $1.125 \times 1.125°$, except for the trajectory calculations, for which we retrieved the model data at a horizontal resolution of $0.5 \times 0.5°$. The trajectories are calculated from the 3-D wind fields from ECMWF with the Lagrangian Trajectory Tool LAGRANTO, developed at the ETH Zurich (Wernli and Davies, 1997).

2.2 Trajectory mapping

Several techniques exist for the construction of synoptic scale constituent maps from one or more time series of point measurements of long lived trace species. Most notable among these techniques are "reverse domain filling" (Dritschel, 1988 and Sutton et al., 1994) and "trajectory mapping" (Pierce et al., 1994 and Morris et al., 1995). Here we apply the trajectory mapping technique to the ground-based H_2O measurements to generate synoptic scale maps of the middle atmospheric H_2O distribution at a given time and altitude layer. For this method, it is required that the H_2O mixing ratio remains constant along the trajectories, i.e. that there is neither mixing with surrounding air masses nor (photo-)chemical processing or phase changes of H_2O. For a trajectory mapped H_2O distribution, we define a target time and pressure layer. Then we take all observations within ± 10 days around the target time and calculate trajectories, starting from each observation point (in altitude and time) and stopping at the target time, going either forward or backward in time. We then choose all the trajectories that end up within the target pressure layer and map the corresponding H_2O observations along the trajectories from the observation time and location to the target time and location.

2.3 The edge of the polar vortex

In the literature, there exist several definitions of the edge of the polar vortex. Chen (1994) defined it as the potential vorticity (PV) contour that has the smallest lengthening rate (WMO, 2003). That is the PV contour whose length has the smallest growth rate over time. Other definitions include the wind maximum, Bowman, 1996) and the strongest PV gradient constrained by the wind maximum (Nash et al., 1996). The latter definition was modified by Manney et al. (2007). They used the maximum of the product of PV gradient and wind speed. For an automated vortex edge detection, they additionally had to include several criteria to prevent misidentification of the vortex, especially at the stratopause, where the PV gradient structure is very complex. PV proved as an accurate variable for the detection of the vortex edge from the lower stratosphere up to the stratopause. However, above approximately 3000 K (60 km) during most of the time, PV is not a vortex-centered coordinate anymore and can thus not

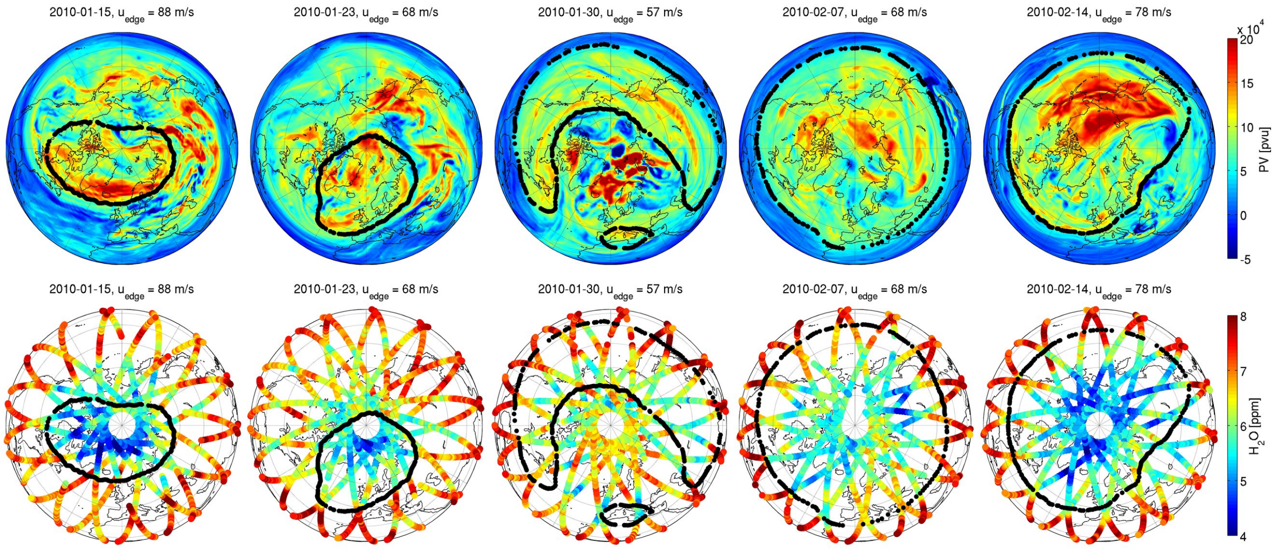

Fig. 1. ECMWF PV (upper panels) and Aura MLS H_2O (lower panels) on the 3300 K isentropic surface (approximately 0.1 hPa) overlaid by the edge of the polar vortex (black contour) during the period of the major SSW in January 2010. PV is given in [pvu], which corresponds to 10^{-6} K m^2 kg^{-1} s^{-1}. H_2O is given in VMR as parts per million [ppm]. Red (blue) colors correspond to relatively high (low) values. Dates from left to right: 15 January, 23 January, 30 January, 7 February and 14 February 2010. The average wind speed along the vortex edge is shown in the caption of the subplots.

be used to determine the polar vortex in the mesosphere (Harvey et al., 2009), even though there still is a strong circulation around the polar low pressure system in the mesosphere. Harvey et al. (2002) introduced a new definition for the vortex edge up to the stratopause by integrating the scalar quantity Q (the ratio between the relative contributions of strain and rotation in a wind field) and wind speed along streamfunction isopleths.

Since we want to interpret the H_2O distribution in the mesosphere as well as in the stratosphere in relation to the polar vortex, we use here a vortex definition that is not based on PV. Hereafter, we divide the mesosphere from the stratosphere by the 1 hPa isobaric level. The definition is partly adapted from the definition of Harvey et al. (2002) by integrating wind speed along contour lines of a certain variable. In this paper, we define the edge of the polar vortex as the geopotential height (GPH) contour on isobaric levels that (a) encircles a low pressure system, (b) is everywhere north of 15° N (i.e. no point of the contour lies southward of 15° N), (c) is longer than 15000 km and (d) has on average the highest absolute wind speed along the GPH contour, compared to the other GPH contours on the same pressure level that also satisfy conditions (a) to (c). The condition (d) only allows one GPH contour (the one with the highest wind speed). However, if there are other contours of the same geopotential height that also satisfy conditions (a) to (c) (e.g. during a split vortex situation), we also use these other contours as edges of weaker vortices in addition to the main vortex edge. Such a definition is valid from the lower stratosphere up to the mesopause.

To illustrate the performance of our definition, we compare it to different tracers for the polar vortex: PV, H_2O, CO and N_2O. Isentropic PV is a good tracer for the polar vortex from the lower stratosphere up to the stratopause, because PV is conserved in adiabatic processes. CO is a good tracer for the vortex at the stratopause and in the mesosphere, as the subsidence inside the vortex transports CO-rich air from above the mesosphere to lower altitudes, leading to substantially higher amounts of CO inside the vortex than outside. H_2O is a good tracer in the mesosphere and the stratosphere, because the subsidence inside the vortex in combination with vertical H_2O gradients leads to different H_2O mixing ratios inside and outside of the vortex (e.g. Lee et al., 2011, and references therein). H_2O cannot be used as a tracer in the altitude region of the H_2O volume mixing ratio (VMR) peak. For the stratosphere, we use N_2O as an indicator of the polar vortex, because N_2O has very low mixing ratios inside the stratospheric vortex and a strong gradient across the vortex edge (Sparling, 2000).

Figure 1 shows ECMWF PV (upper panels) and Aura MLS H_2O (lower panels) on the 3300 K isentropic surface (approximately 0.1 hPa) on five dates in the course of the major SSW. Superposed are the vortex edge contours on the same isentropic surface. Since the edge of the vortex is calculated on isobaric surfaces, the vortex edge on an isentropic surface as in Fig. 1 is shown as crossing points between the (isobaric) vortex edge with the 3300 K isentropic surface. As visible in the H_2O distribution, our definition of the edge of the vortex performs best before the SSW, i.e. during quiet periods: Low H_2O values are found within the vortex and high

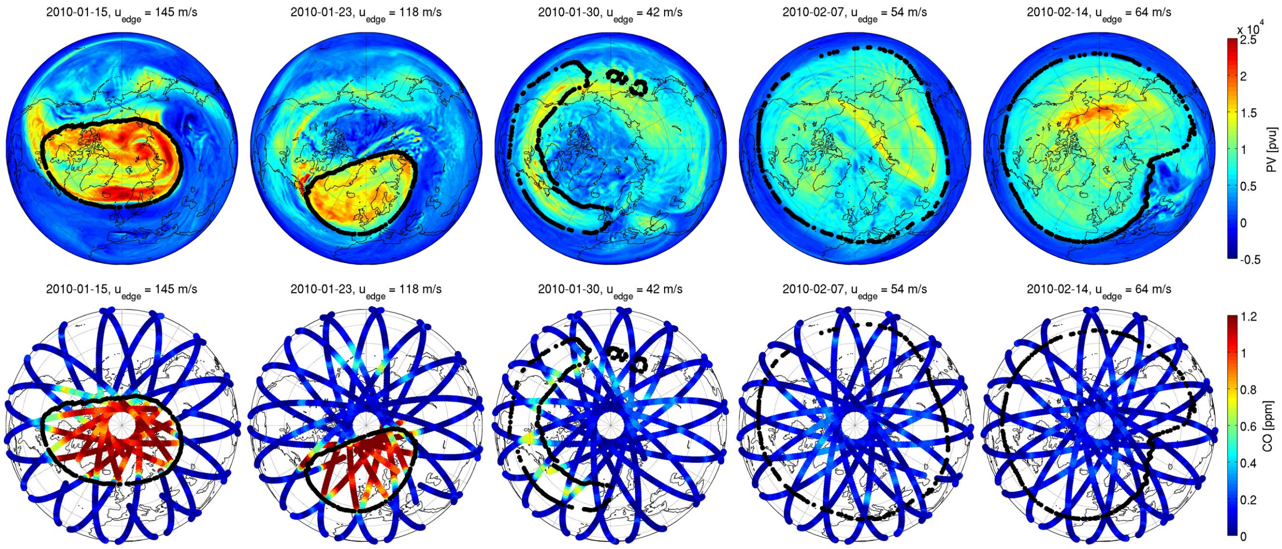

Fig. 2. As in Fig. 1, but on the 1800 K isentropic surface (approximately 1 hPa) and showing Aura MLS CO VMR [ppm] instead of H_2O in the lower panel.

values outside, as expected. During and after the SSW, the vortex edge still encloses low H_2O values, although the edge of the vortex seems to be too far South over the Pacific region. This could be due to deficiencies of the performance of the ECMWF analysis in the mesosphere during SSWs or due to enhanced mixing across the vortex edge due to the weakening of the vortex (the wind speed along the vortex edge decreased from 88 m s^{-1} before the SSW to 57 m s^{-1} during the SSW). From the PV distribution (upper panels), it is visible that PV is not vortex-centered in the mesosphere (which was pointed out by Harvey et al., 2009).

In the stratopause region, we compare our vortex edge definition with PV and CO (Fig. 2, analogous to Fig. 1, but showing everything on the 1800 K isentropic surface (approximately 1 hPa) and CO instead of H_2O). In this altitude region, PV is vortex-centered and thus agrees well with our vortex edge definition. However, small scale structures (such as PV filaments) are not captured by our definition of the vortex edge. Before the SSW, horizontal gradients in PV and CO agree well with the vortex edge. Even during the SSW, the vortex edge encloses the region of high CO and high PV. Although the vortex broke down at this altitude (wind speed along the vortex edge dropped from 145 m s^{-1} before the SSW to 42 m s^{-1} during the SSW), our definition still performs well. After the SSW, CO is well-mixed across the Northern Hemisphere and remains very low while the vortex reformed at low latitudes. The subsidence inside the vortex first needs to transport CO-rich air from higher altitudes towards the stratopause region before CO can again be used as a tracer for the vortex at this altitude.

In the stratosphere (Fig. 3, analogous to Fig. 1, but showing everything on the 800 K isentropic surface (approximately 10 hPa) and N_2O instead of H_2O), PV and the vortex edge by our definition agree very well (upper panels). Even the vortex split after the SSW, visible in PV and N_2O, is captured by our definition. The comparison with N_2O (lower panels) also shows good agreement (i.e. the lowest N_2O values are located within the vortex), even during and after the SSW.

As shown by Figs. 1 to 3, our definition for the edge of the polar vortex performs well from the stratosphere up to the mesosphere, even during a SSW. Further, our definition isolates the polar vortex from small scale PV filaments at the vortex edge. However, since there is no threshold for a lowest wind speed, this definition always yields a vortex edge (as long as there is a low pressure system northward of 15° N), even for very weak vortices. Therefore, the strength of the vortex (expressed by the wind speed at the edge) is also considered in the analysis of the temporal evolution of the polar vortex.

3 The polar vortex during the SSW

To describe the major SSW of January 2010, we begin with the temporal evolution of the zonal mean temperature and zonal mean zonal wind between mid-November 2009 and mid-March 2010. Figure 4 shows the zonal mean temperature from Aura MLS (left panels) and the zonal mean zonal wind from ECMWF (right panels) on 0.1 (top) and 10 hPa (bottom) against latitude and time. In the stratosphere (10 hPa), a strong negative temperature gradient was present during December and January from 45° N towards the North Pole due to the polar vortex. This gradient reversed at the end of January, when the zonal mean temperature in the polar

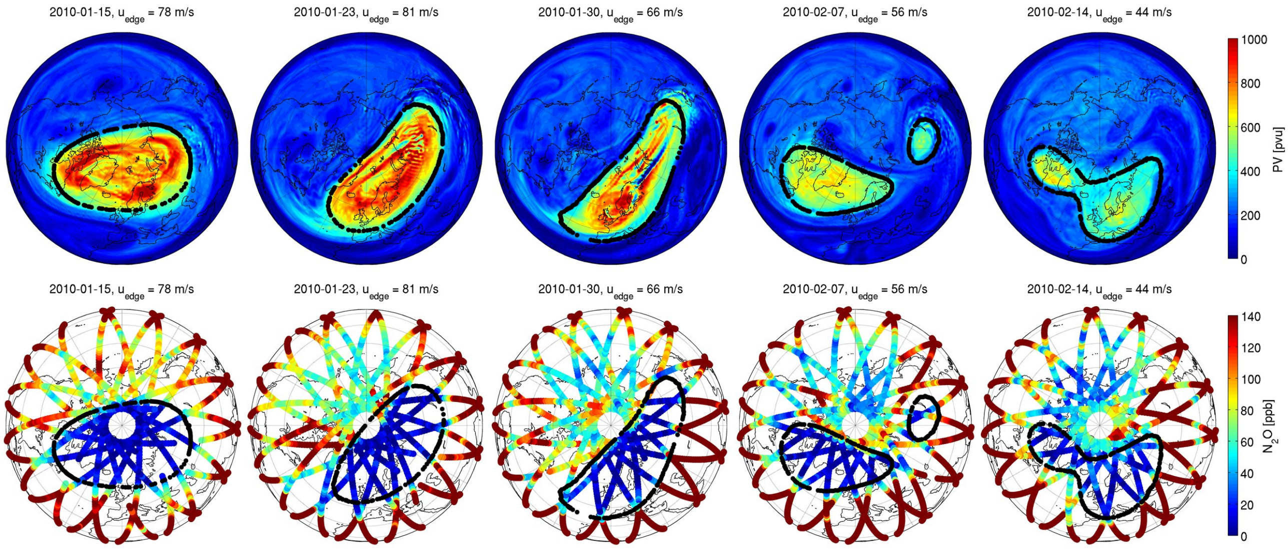

Fig. 3. As in Fig. 1, but on the 800 K isentropic surface (approximately 10 hPa) and showing Aura MLS N_2O VMR [parts per billion, ppb] instead of H_2O in the lower panel.

region increased by approximately 25 K within a few days. At the same time, the zonal mean zonal wind reversed on the two shown pressure levels. The fast increase in zonal mean temperature, the positive latitudinal gradient in the zonal mean temperature on 10 hPa and the reversal of the zonal mean zonal wind on 10 hPa northward of 60° N define this event as a major sudden stratospheric warming, starting approximately on 26 January 2010, which is hereinafter referred to as the beginning of the SSW. In the stratosphere, the strong negative temperature gradient towards the pole from before the major SSW did not recover after the major SSW, i.e. the polar vortex did not re-form to its original strength at this pressure level (10 hPa). As evident in the figure, there was also a cooling in the mesosphere in the polar region north of 60° N during the major SSW. The mesospheric cooling during the SSW was followed by a slow warming from the beginning of February until mid-March.

For the interpretation of our ground-based observations, it is important to consider the development of the polar vortex at different altitudes with respect to the measurement locations. Figure 5 shows the edge of the polar vortex from approximately 20 to 80 km altitude on four dates: 23 January (before the SSW), 31 January (during the SSW), 7 February and 14 February (after the SSW). The upper panel shows projections of the vortex edge contours where the colors indicate the altitude of the respective contour lines. The lower panels show the corresponding 3-D representation where the colors indicate the average wind speed along the vortex edge contours. The geographical locations of the three observation sites are indicated in the top panels by a cross for Bern, a diamond for Onsala and a circle for Sodankylä, and in the lower panel by vertical lines (black for Bern, magenta for Onsala and green for Sodankylä).

Before the SSW, on 23 January, the stratospheric vortex was located above Northern Europe and Asia and tilted towards the southwest with height. The vortex area decreased slightly from the lower stratosphere to the upper stratosphere. From the stratopause to the upper mesosphere, the vortex area expanded westward towards North America. The vortex was strongest in the stratopause region with westerly wind speeds exceeding $100\,\mathrm{m\,s^{-1}}$. Of the three measurement sites, only Sodankylä was located inside the vortex at all altitudes. Onsala was outside of the vortex in the lower stratosphere below 24 km altitude and Bern was outside of the vortex in the lower and middle stratosphere (below approximately 31 km).

During the SSW on 31 January, the stratospheric vortex moved further away from the pole towards Europe and stretched towards Asia. With height, the vortex was tilted westward and the vortex area and strength decreased compared to lower altitudes (Fig. 5, second panel). Near the stratopause, wind speeds at the vortex edge decreased from more than $100\,\mathrm{m\,s^{-1}}$ on 23 January to approximately $30\,\mathrm{m\,s^{-1}}$ on 31 January. Above the stratopause, the vortex shifted to the region of the North Pacific and East Asia and weakened by 50 % in terms of wind speed. The strongest wind speeds at this time were $60\,\mathrm{m\,s^{-1}}$ and located in the middle stratosphere at approximately 30 km. Hence, the major SSW was accompanied by a shift of the stratospheric vortex towards Europe, a significant deceleration of the vortex throughout the middle atmosphere and a geographical separation between the stratospheric and the mesospheric vortex. The three measurement locations lay inside the stratospheric vortex, but outside of the mesospheric vortex. Considering

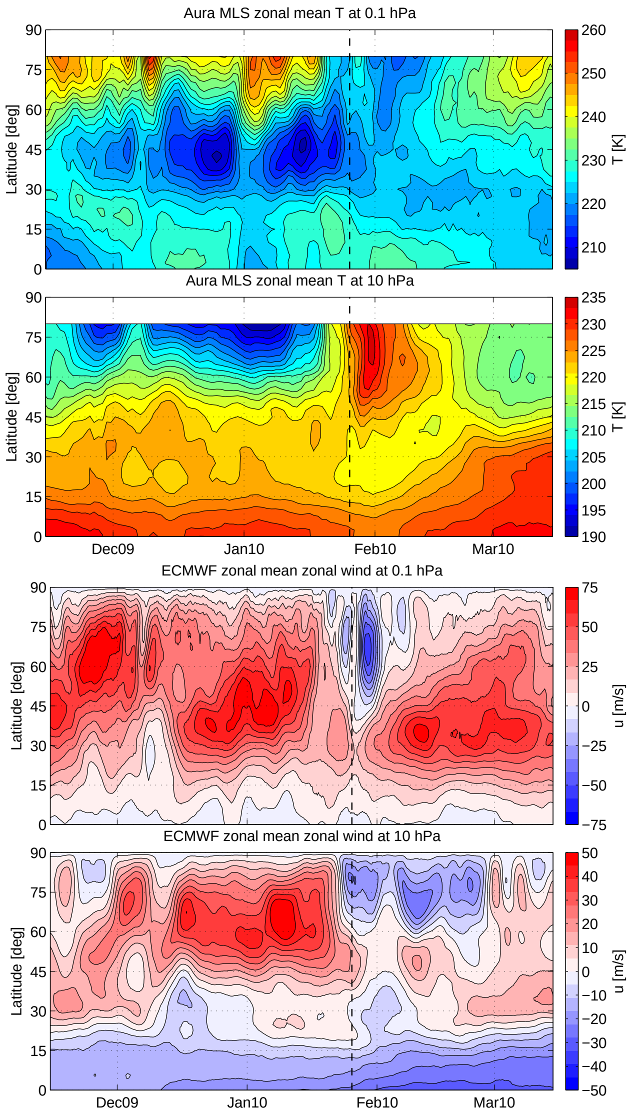

Fig. 4. Latitude-time cross sections of the zonal mean temperature [K] from Aura MLS (upper panels) and zonal mean zonal wind [$m\,s^{-1}$] from ECMWF (lower panels) during northern winter 2009/2010 at 0.1 and 10 hPa. Date markers indicate the first day of the month. The black dashed line indicates the beginning of the major SSW in the stratosphere. In the zonal wind plots, red (blue) colors correspond to eastward (westward) wind.

the strong decrease in wind speed at the vortex edge, we can say that the vortex broke down during the SSW above approximately 50 km.

Eight days later, on 7 February, the vortex in the lower stratosphere was long and narrow and located over Greenland, Northern Europe and Asia, while in the middle stratosphere, the vortex split into two parts, one smaller part over central Russia and one larger part over Greenland and Scandinavia. In the upper stratosphere, the smaller part of the vortex disappeared and the larger part decreased in area. In the mesosphere, a new, pole-centered vortex formed at approximately 40° N with westerly wind speeds increasing in altitude. Hence at that time, all three measurement sites were located within the new mesospheric vortex. In the lower and middle stratosphere, only Sodankylä was situated within the vortex.

On 14 February, the mesospheric vortex gained in strength and was still different in shape compared to the vortex in the stratosphere. In the lower stratosphere, the long and narrow vortex from 7 February had split into two vortices. The split vortex recombined in the upper stratosphere, where it was located over Europe, Southern Greenland and the Northeast of Canada. The three measurement sites lay within the vortex throughout the middle atmosphere.

As seen in Fig. 5, the evolution of the polar vortex during the time of the SSW was different on every pressure level. After the SSW, the mesosphere and the stratosphere behaved completely different. The following section relates the evolution of the vortex to the evolution of the H_2O and O_3 profiles monitored by the network of ground-based microwave radiometers.

4 H_2O and O_3 observations in relation to the polar vortex

Figure 6 shows measurements from the four ground-based microwave radiometers at the three measurement locations from December 2009 until March 2010. Panel (a) shows GROMOS O_3 measurements in Bern, (b) shows MIAWARA H_2O measurements in Bern, (c) shows H_2O measurements in Onsala and (d) shows MIAWARA-C H_2O measurements in Sodankylä. The stratopause, i.e. the height of the temperature maximum (from Aura MLS), is indicated by the thick black dashed line. The thick black and magenta contour lines show the vortex edge crossings over the measurement locations, while going from magenta to black means that the vortex moves over the measurement location and from black to magenta means that the vortex moves away from the measurement location. These contour lines are drawn when the vortex edge is located at a distance of 100 km from the measurement locations (black (magenta) contours are drawn when the measurement location lies inside (outside) the vortex). The thin black and magenta contours are drawn when the vortex edge is located at a distance of 500 km from the measurement location. By drawing also these thin contours, one can see when the vortex was in the near vicinity of the measurement locations, but the vortex edge did not actually cross the measurement location (e.g. Fig. 6a and b (Bern) between 7 and 50 hPa in mid-December and the beginning of January).

To better explain this vortex edge visualization with an example, we use the O_3 time series from GROMOS in Bern (Fig. 6a) on 10 hPa. In the middle of January, O_3 VMR on 10 hPa was relatively high and the stratospheric polar vortex was not located over Bern, because the next vortex edge

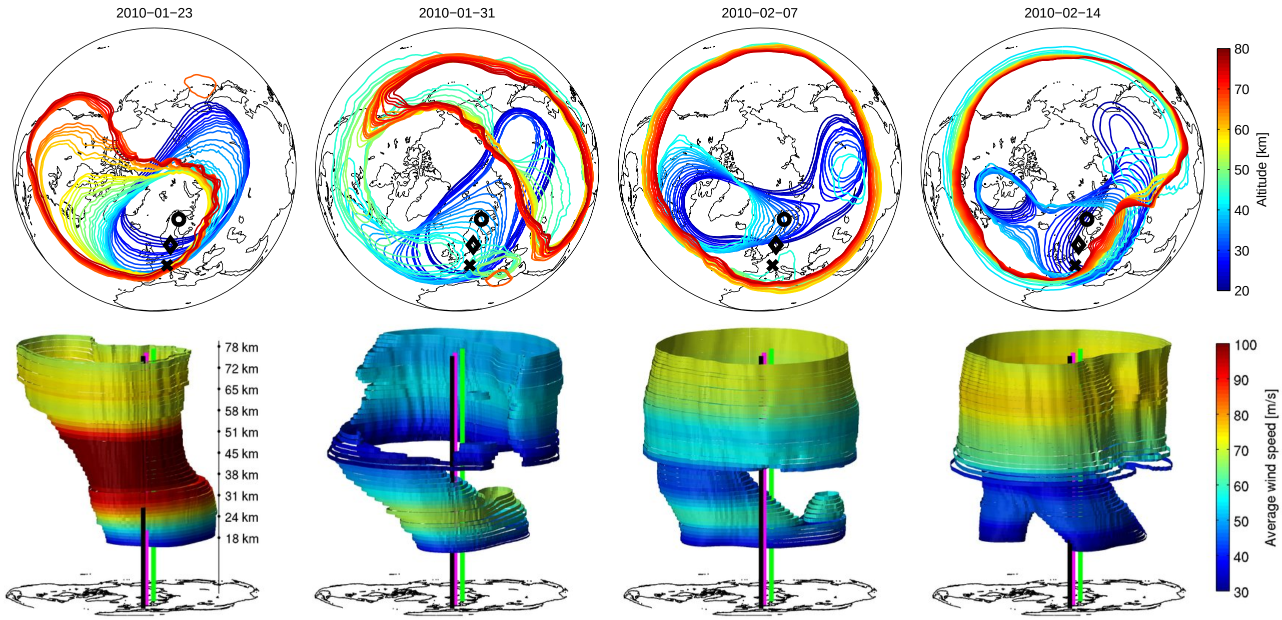

Fig. 5. Upper panel: projections of the edge of the polar vortex for 23 January, 31 January, 7 February and 14 February 2010 (from left to right). Colors indicate the geopotential height in [km]. The black cross indicates Bern, the black diamond Onsala and the black circle Sodankylä. Lower panel: corresponding 3-D representation of the polar vortex. The colors indicate average wind speed [m s^{-1}] along the vortex edge. The vertical black line indicates Bern, the magenta line Onsala and the green line Sodankylä.

crossing at this pressure level is from magenta to black, i.e. from outside-vortex to inside-vortex, on 26 January. Coinciding with the onset of the SSW in the stratosphere, the vortex moved over Bern and O_3 decreased by approximately 30 %. The next vortex edge crossing happens on 3 February with the contours changing from black to magenta, i.e. from inside-vortex to outside-vortex, and O_3 increased again. On 10 February, the vortex moved back to Bern (magenta to black contours) and O_3 decreased again. On 20 February, the vortex moved away from Bern followed by an O_3 increase.

The stratospheric H_2O observations by MIAWARA in Bern (Fig. 6b) also showed agreement with the vortex location between 10 and 4 hPa. With the beginning of the major SSW, stratospheric H_2O increased, coinciding with the vortex shift over Bern. After 3 February, the vortex moved away from Bern and H_2O decreased. Until 9 February, H_2O remained low and when the vortex came back on 10 February, H_2O increased again. By the end of February and the beginning of March, the vortex moved again away from Bern and relatively low H_2O values were observed during that time. The middle stratospheric H_2O and O_3 observations above Bern are well anti-correlated and both agree with the location of the polar vortex with respect to Bern. However, the agreement of the composition measurements and the location of the polar vortex breaks down in the stratopause region (around 1 hPa). In the mesosphere, H_2O also shows agreement with the movement of the vortex, but to a lesser extent than in the stratosphere. Between mid-December and the end of 2009, low H_2O was observed around 0.1 hPa and Bern was within the mesospheric vortex. In the first half of January, Bern was not located inside the mesospheric vortex, until just before the onset of the major SSW at the end of January, the mesospheric vortex was again over Bern for a few days, correlating with low H_2O values. After 1 February, Bern lay within the newly formed mesospheric vortex until mid-March with one short exception in the middle of February. During that time period, mesospheric H_2O continuously decreased, showing the subsidence of air inside the re-formed vortex.

There are many data gaps in the H_2O observations from Onsala (Fig. 6c), but nevertheless, the observations agree with the relative location of the polar vortex. At the end of January, i.e. during the SSW, relatively high mesospheric H_2O mixing ratios were observed over Onsala, approximately 50 % higher than during the last measurement before the SSW, on 5 January. While the mesospheric vortex was over Onsala at the beginning of January, the vortex broke down at the end of January, coinciding with the high H_2O values and the onset of the SSW. From 1 February until mid-March, the re-formed mesospheric vortex and the subsequent descent inside the vortex lead to decreasing mesospheric H_2O mixing ratios over Onsala.

The situation in Sodankylä (Fig. 6d) was similar to Onsala. MIAWARA-C observed low H_2O above 3 hPa before the SSW. Exactly at the beginning of the SSW, mesospheric H_2O increased by approximately 40 % between 3 and 0.07 hPa,

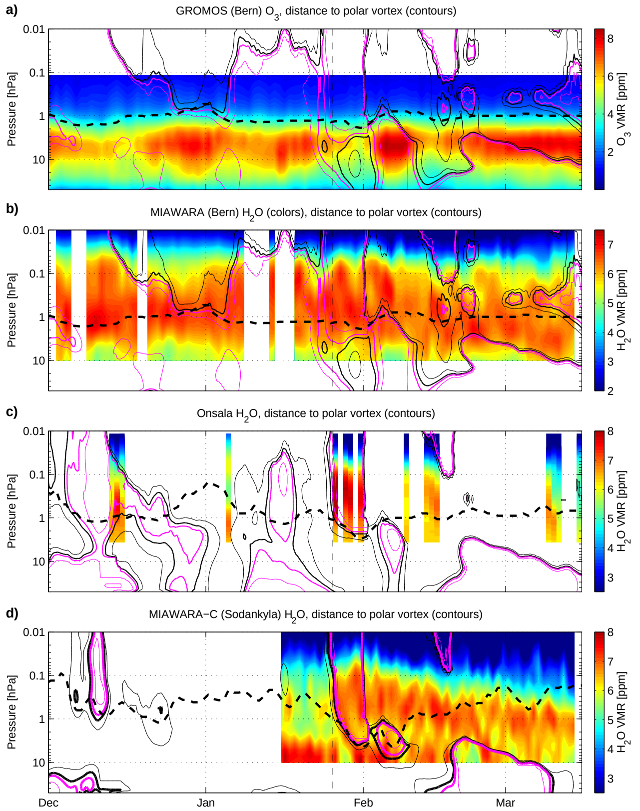

Fig. 6. Ground-based radiometer measurements of O_3 and H_2O during winter 2009/2010. **(a)** GROMOS O_3 VMR in Bern. **(b)** MIAWARA H_2O VMR in Bern. **(c)** H_2O VMR in Onsala. **(d)** MIAWARA-C H_2O VMR in Sodankylä. Units are ppm. Red (blue) colors correspond to relatively high (low) values. The contour lines indicate when the polar vortex crossed the measurement location (see text for details). The vertical black dashed line indicates the beginning of the major SSW in the stratosphere. The thick dashed black line indicates the stratopause (obtained from the temperature maximum in Aura MLS temperature data).

coinciding with the polar vortex that moved away from Sodankylä and eventually broke down. During the SSW, the stratopause dropped by approximately one pressure decade from 0.3 to 4 hPa. On 1 February, the mesospheric vortex reformed, Sodankylä remained inside the mesospheric vortex until mid-March and the observed H_2O mixing ratios continually decreased until mid-March. The H_2O decrease indicates the descent of dry mesospheric air in the polar region. This subsidence was also observed in the stratosphere at around 3 hPa just before the SSW. A detailed study on this particular observation of mesospheric subsidence can be found in Straub et al. (2012). On 20 February, relatively low stratospheric H_2O was observed between 10 and 3 hPa for approximately 5 days, coinciding with the shift of the vortex away from Sodankylä. However at the end of February, high H_2O was observed while the stratospheric vortex was still absent from Sodankylä. The reason for this observed change in H_2O is likely associated with an artifact in the retrieved profile due to baseline issues of the instrument.

5 Trajectory Mapping of H_2O during the SSW

As H_2O is a good tracer for the polar vortex in the lower and middle stratosphere and the mesosphere, we are interested in how much of the evolution of the mesospheric and stratospheric vortex can be represented by the data from ground-based measurement locations. In addition we explore the information content of the regional observations for the derivation of synoptic maps of trace gases. In Figs. 7 and 8, we show the application of the trajectory mapping technique (as described in Sect. 2.2) on our H_2O observations from MIAWARA (Bern) and MIAWARA-C (Sodankylä). The data from Onsala are not used in the trajectory mapping because they are sparse and they seem to have a strong bias to the data from the other two instruments. We focus on two pressure layers, one in the mesosphere between 0.14 and 0.07 hPa and one in the stratosphere between 14 and 7 hPa. Since the vortex structure can change significantly over short vertical distances (as visible in Fig. 5), the chosen pressure layer width of approximately 6 km is a trade-off between minimizing the layer width and maximizing the number of data points (i.e. the number of trajectories that end up within the pressure layer). In additon to the H_2O maps from the trajectory mapping, we also show direct H_2O measurements from Aura MLS for a comparison.

The left column of Fig. 7 shows the trajectory mapped ground-based H_2O observations between 0.14 and 0.07 hPa for the mesosphere on the same dates as in Fig. 5. In addition, we show the edge of the polar vortex on four pressure levels within 0.14 and 0.07 hPa. The direct H_2O measurements of Aura MLS averaged over the same pressure layer and on the same dates are shown in the right column. Before the SSW (Fig. 7a and b), the region of low H_2O VMR is concentrated in the Northwest of Europe and the Northeast of North America. The low H_2O VMR is typical for inside the mesospheric vortex and shows the subsidence of dry upper mesospheric air to lower levels during winter time. The vortex edge contour follows the H_2O gradient in most parts. However, the low water vapor over the Northeast of North America seen in the trajectory mapped data (right column) is neither reflected by the location of the vortex nor by the direct H_2O measurements (left column). Since the trajectory mapped data points are at a specific pressure level within the pressure layer in question, but the Aura MLS data are averaged over the whole pressure layer, the low H_2O feature over North America in the trajectory mapped data could be a real feature, covering a narrow vertical range, but is smoothed out in the averaged MLS data. During the SSW, on 31 January, the mesospheric vortex moved towards Asia and the North Pacific region, but was very weak, as was seen in Fig. 5. This was accompanied by large scale mixing of H_2O-rich, midlatitudinal air with

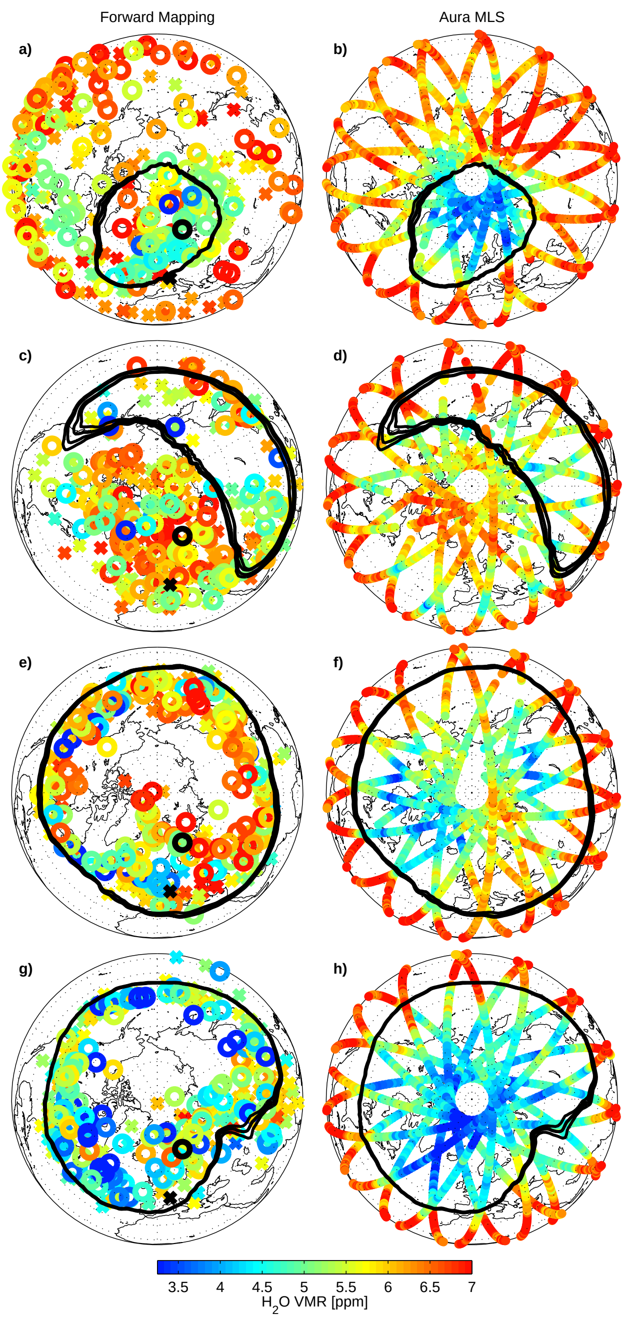

Fig. 7. H_2O VMR within 0.14 and 0.07 hPa (approximately 61 to 67 km altitude). Left column: trajectory mapped ground-based H_2O observations from Bern (crosses) and Sodankyla (circles). The black cross and circle indicate the location of MIAWARA (Bern) and MIAWARA-C (Sodankylä), respectively. Right column: H_2O measurements from Aura MLS v3.3, averaged between 0.14 and 0.07 hPa. Red (blue) colors correspond to relatively high (low) H_2O values. Units are ppm. The black contours indicate the edge of the polar vortex on four pressure levels within 0.14 and 0.07 hPa. Dates are (from top to the bottom) 23 January **(a, b)**, 31 January **(c, d)**, 7 February **(e, f)** and 14 February 2010 **(g, h)**.

dry, polar air. This explains the well-mixed H_2O distribution in the mesosphere at midlatitudes and in the polar region during the SSW. After the SSW (7 February, Fig. 7e and f), the mesospheric vortex re-formed northward of 40° N, and the H_2O distribution remained well-mixed. Nearly all trajectory mapped H_2O observations originated from inside the newly formed vortex. Therefore it is not possible to determine the regions with enhanced or reduced H_2O VMR from the trajectory mapped data. However, the direct satellite measurements show that H_2O VMR inside the vortex is lower than outside. The last plot on 14 February (Fig. 7g and h) shows that H_2O decreased compared to directly after the SSW (in both data sets), indicating the large scale descent of mesospheric air, which is also seen in the H_2O time series in Fig. 6, especially in the time series from MIAWARA-C in Sodankylä.

For the trajectory mapped stratospheric H_2O distribution, plots analogous to Fig. 7 are shown in Fig. 8 for a pressure layer around 14 and 7 hPa. There are less data points than in the mesospheric equivalent plots because 10 hPa is approximately the lower measurement limit of the two radiometers. Just before the SSW (Fig. 8a and b), there are many trajectory mapped data points with high H_2O values in the north of Europe and Asia, surrounded by data points with relatively low H_2O values. The trajectory mapping correctly determines the region of the relatively "humid" polar vortex, as compared to the vortex edge and the direct measurements. However, a precise distinction between inside and outside of the vortex is not possible with the trajectory mapped H_2O data alone. On 31 January, most of the high H_2O values are located inside the vortex while most of the low H_2O values are located outside. There are some outliers (very low values inside the vortex over Scandinavia) originating from MIAWARA-C that disturb the overall picture. Eight days later, on 7 February (Fig. 8e and f), the trajectory mapped H_2O distribution indicates the vortex split at that time. Nearly all low H_2O values occur outside the vortex and the high H_2O values are inside the vortex. On 14 February, the two vortices merged again (Fig. 8g and h). The agreement between H_2O and vortex is visible, but not as clear as on 7 February.

Compared to direct measurements of H_2O by Aura MLS, the synoptical maps from the trajectory mapping are much more noisy and some regions are not covered. For example, the (weak) mesospheric vortex on 31 January (Fig. 7c) was only sampled with very little data points from the trajectory mapping and the center of the re-formed vortex after the SSW (Fig. 7e and g) was not sampled at all with the trajectory mapping technique. Thus, inhomogenous H_2O distributions within the vortex cannot be captured with only two ground-based measurement locations. Discrepancies between trajectory mapped and direct observations can arise from the way the two data sets are compared (forward mapped data at one specific pressure level vs. direct measurements average over the given pressure layer), from errors in the retrieval process of the ground-based observations and from the trajectory calculations that require accurate knowledge of the wind field.

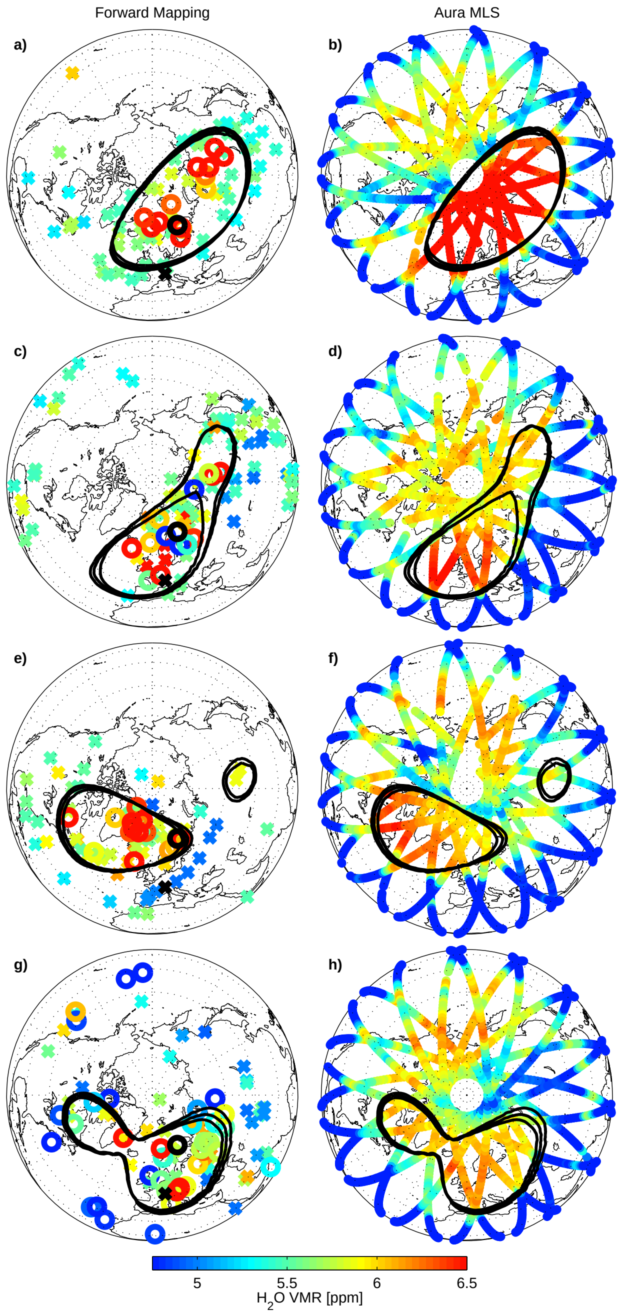

Fig. 8. Same as Fig. 7, but for a pressure layer between 14 and 7 hPa.

A further problem that affects the quality of the trajectory mapping with data from an instrument network are biases between the different instruments, which usually depend on altitude and/or time, resulting in a combined data set that is not homogenized. Because the lower limit of our microwave radiometers is 10 hPa and the retrieval at this pressure level can be strongly influenced by baselines in the spectrum, the trajectory mapping in the stratosphere did not perform as well as in the mesosphere. A better validation of the trajectory mapping method would be a quantitative analysis of points of trajectory mapped data and satellite measurements that are coincident within some reasonable criteria in all three directions. Such an analysis was not (yet) done. However, the example shows that ground-based observations of a radiometer network can provide valuable synoptical maps of trace gases when trajectory mapping is applied.

6 Summary

In this study we presented H_2O and O_3 observations from ground-based microwave radiometers located across Europe during northern winter 2009/2010. A major SSW occurred at the end of January 2010. We described the temporal evolution of the zonal mean temperature, zonal mean zonal wind and the polar vortex during the SSW throughout the middle atmosphere. In order to determine the edge of the polar vortex, we used a definition based on geopotential height and maximum wind speed in order to create a consistent picture of the polar vortex from the lower stratosphere to the upper mesosphere. This definition successfully determines the edge of the vortex throughout the middle atmosphere, which is shown by a comparison to ECMWF PV and trace gases from Aura MLS. In the course of the SSW, the stratospheric vortex shifted towards Europe and Asia and tilted westward with height. The mesospheric vortex broke down. After the SSW, a split of the vortex occurred in the stratosphere while the mesospheric vortex re-formed in the area from 40° N to 90° N.

The ground-based observations of H_2O and O_3 are interpreted in terms of the location of the polar vortex with respect to the measurement locations. Both the observed H_2O and O_3 VMR are largely influenced by the position of the vortex. Stratospheric O_3 over Bern decreased by approximately 30 % when the vortex moved over Bern. The agreement between the local H_2O observations and the position of the vortex is strongest in the stratosphere and the mesosphere, where H_2O is as a good tracer for atmospheric transport processes and dynamics. Also visible in the H_2O observations, in particularly at Sodankylä, is the subsidence of mesospheric air into the stratosphere that was disrupted during the SSW.

We used trajectory mapping to combine the H_2O observations from the three locations into a synoptic scale map of the H_2O distribution in the Northern Hemisphere. The trajectory mapped ground-based data allowed determining the approximate position and extent of the vortex in the stratosphere. In the mesosphere, the region of the large scale descent before the SSW, the breakdown of the vortex during the SSW and the continued subsidence afterwards can be seen to some extent in the trajectory mapped observations (but clearly not as precise as in direct satellite measurements). Trajectory mapping of ground-based observations may prove to be a useful tool, and the present study demonstrates the potential of a network of ground-based instruments for the derivation of synoptical maps of trace gases in the middle atmosphere. Improvements in the trajectory mapping method could be done by correcting the biases between the different instruments (homogenization of the network) and by using more instruments over a broad geographical range. Within NDACC, there are half a dozen of H_2O radiometers suitable for combining by trajectory mapping. Of course, the ground-based network cannot be a substitute for satellite measurements. Both data sources are complementary in the nature of their measurements and should be used together.

Acknowledgements. This work has been funded by the Swiss National Science Foundation under grant 200020-134684, MeteoSwiss in the frame of the project MIMAH, the Sodankylä LAPBIAT-2 campaign and the Oeschger Centre for Climate Research. We thank the COST Action ES604 WaVaCS. We acknowledge ECMWF for the data access of the operational analysis data and NASA for the data access of Aura MLS. We also thank Simone Studer for providing the ozone data from the GROMOS radiometer. Finally, we would like to thank the anonymous referees for their critical review that helped to improve this paper.

Edited by: W. Lahoz

This publication is supported by COST – www.cost.eu

References

Allen, D. R., Stanford, J. L., Nakamura, N., Lopez-Valverde, M. A., Lopez Puertas, M., Taylor, F. W., and Remedios, J. J.: Antarctic polar descent and planetary wave activity observed in ISAMS CO from April to July 1992, Geophys. Res. Lett., 27, 665–668, doi:10.1029/1999GL010888, 2000.

Bowman, K. P.: Rossby wave phase speeds and mixing barriers in the stratosphere, J. Atmos. Sci., 53, 905–916, 1996.

Calisesi, Y., Wernli, H., and Kämpfer, N.: Midstratospheric ozone variability over Bern related to planetary wave activity during the winters 1994–1995 to 1998–1999, J. Geophys. Res., 106, 7903–7916, 2001.

Charlton, A. J. and Polvani, L. M.: A new look at stratospheric sudden warmings. Part I: Climatology and modeling benchmarks, J. Climate, 20, 449–469, 2007.

Chen, P.: The permeability of the Antarctic vortex edge, J. Geophys. Res., 99, 20563–20571, 1994.

De Wachter, E., Hocke, K., Flury, T., Scheiben, D., Kämpfer, N., Ka, S., and Oh, J. J.: Signatures of the Sudden Stratospheric Warming events of January - February 2008 in Seoul, S. Korea, Adv. Space Res., 48, 1631–1637, doi:10.1016/j.asr.2011.08.002, 2011.

Deuber, B., Haefele, A., Feist, D. G., Martin, L., Kämpfer, N., Nedoluha, G. E., Yushkov, V., Khaykin, S., and Kivi, R .and Vömel, H.: MIddle Atmospheric WAter vapour RAdiometer (MIAWARA): Validation and first results of the LAUTLOS/WAVVAP campaign, J. Geophys. Res., 110, D13306, doi:10.1029/2004JD005543, 2005.

Dritschel, D. G.: Contour surgery: A topological reconnection scheme for extended integrations using contour dynamics, J. Comput. Phys., 77, 240–266, 1988.

Fisher, M., O'Neill, A., and Sutton, R.: Rapid descent of mesospheric air into the stratospheric polar vortex, Geophys. Res. Lett., 20, 1267–1270, doi:10.1029/93GL01104, 1993.

Flury, T., Hocke, K., Haefele, A., Kämpfer, N., and Lehmann, R.: Ozone depletion, water vapor increase, and PSC generation at midlatitudes by the 2008 major stratospheric warming, J. Geophys. Res., 114, D18302, doi:10.1029/2009JD011940, 2009.

Forkman, P., Eriksson, P., and Winnberg, A.: The 22 GHz radioaeronomy receiver at onsala space observatory, J. Quant. Spectrosc. Ra., 77, 23–42, doi:10.1016/S0022-4073(02)00073-0, 2003.

Goncharenko, L. P., Coster, A. J., Chau, J. L., and Valladares, C. E.: Impact of sudden stratospheric warmings on equatorial ionization anomaly, J. Geophys. Res., 115, 1–11, doi:10.1029/2010JA015400, 2010.

Haefele, A., De Wachter, E., Hocke, K., Kämpfer, N., Nedoluha, G. E., Gomez, R. M., Eriksson, P., Forkman, P., Lambert, A., and Schwartz, M. J.: Validation of ground based microwave radiometers at 22 GHz for stratospheric and mesospheric water vapor, J. Geophys. Res., 114, D23305, doi:10.1029/2009JD011997, 2009.

Harvey, V. L., Randall, C. E., and Hitchman, M. H.: Breakdown of potential vorticity–based equivalent latitude as a vortex-centered coordinate in the polar winter mesosphere, J. Geophys. Res., 114, 1–12, doi:10.1029/2009JD012681, 2009.

Harvey, V. L., Pierce, R. B., and Hitchman, M. H.: A climatology of stratospheric polar vortices and anticyclones, J. Geophys. Res., 107, 4442, doi:10.1029/2001JD001471, 2002.

Labitzke, K. and Kunze, M.: On the remarkable Arctic winter 2008/2009, J. Geophys. Res., 114, D00I02, doi:10.1029/2009JD012273, 2009.

Lahoz, W. A., Errera, Q., Viscardy, S., and Manney, G. L.: The 2009 stratospheric major warming described from synergistic use of BASCOE water vapour analyses and MLS observations, Atmos. Chem. Phys., 11, 4689–4703, doi:10.5194/acp-11-4689-2011, 2011.

Lee, J. N., Wu, D. L., Manney, G. L., Schwartz, M. J., Lambert, A., Livesey, N. J., Minschwander, K. R., Pumphrey, H. C., and Read, W. G.: Aura Microwave Limb Sounder observations of the polar middle atmosphere: Dynamics and transport of CO and H_2O, J. Geophys. Res, 116, D05110, doi:10.1029/2010JD014608, 2011.

Manney, G. L., Zurek, R. W., O'Neill, A., and Swinbank, R.: On the motion of air through the Stratospheric Polar Vortex, J. Atmos. Sci., 51, 2973–2994, 1994.

Manney, G. L., Daffer, W. H., Strawbridge, K. B., Walker, K. A., Boone, C. D., Bernath, P. F., Kerzenmacher, T., Schwartz, M. J., Strong, K., Sica, R. J., Krüger, K., Pumphrey, H. C., Lambert, A., Santee, M. L., Livesey, N. J., Remsberg, E. E., Mlynczak, M. G., and Russell III, J. R.: The high Arctic in extreme winters: vortex, temperature, and MLS and ACE-FTS trace gas evolution, Atmos. Chem. Phys., 8, 505–522, doi:10.5194/acp-8-505-2008, 2008a.

Manney, G. L., Krüger, K., Pawson, S., Minschwaner, K., Schwartz, M. J., Daffer, W. H., Livesey, N. J., Mlynczak, M. G., Remsberg, E. E., Russell, J. M., and Waters, J. W.: The evolution of the stratopause during the 2006 major warming: Satellite data and assimilated meteorological analyses, J. Geophys. Res., 113, 1–16, doi:10.1029/2007JD009097, 2008b.

Manney, G. L., Daffer, W. H., Zawodny, J. M., Bernath, P. F., Hoppel, K. W., Walker, K. A., Knosp, B. W., Boone, C., Remsberg, E. E., Santee, M. L., Harvey, V. L., Pawson, S., Jackson, D. R., Deaver, L., McElroy, C. T., McLinden, C. A., Drummond, J. R., Pumphrey, H. C., Lambert, A., Schwartz, M. J., Froidevaux, L., McLeod, S., Takacs, L. L., Suarez, M. J., Trepte, C. R., Cuddy, D. C., Livesey, N. J., Harwood, R. S., and Waters, J. W.: Solar occultation satellite data and derived meteorological products: Sampling issues and comparisons with Aura Microwave Limb Sounder, J. Geophys. Res., 12, D24S50, doi:10.1029/2007JD008709, 2007.

Manney, G. L., Schwartz, M. J., Krüger, K., Santee, M. L., Pawson, S., Lee, J. N., Daffer, W. H., Fuller, R. A., and Livesey, N. J.: Aura Microwave Limb Sounder observations of dynamics and transport during the record breaking 2009 Arctic stratospheric major warming, Geophys. Res. Lett., 36, L12815, doi:10.1029/2009GL038586, 2009.

Martius, O., Polvani, L. M., and Davies, H. C.: Blocking precursors to stratospheric sudden warming events, Geophys. Res. Lett., 36, L14806, doi:10.1029/2009GL038776, 2009.

Matsuno, T.: Dynamical model of stratospheric sudden warming, J. Atmos. Sci., 28, 1479–1494, 1971.

McInturff, R.: Stratospheric warmings: Synoptic, dynamic and general-circulation aspects, Tech. Rep. NASA-RP-1017, NASA Reference Publ., Washington, DC, 1978.

Morris, G. A., Schoeberl, M. R., Sparling, L. C., Newman, P. A., Lait, L. R., Elson, L., Waters, J., Suttie, R. A., Roche, A., Kumer, J., and Russell, J. M.: Trajectory Mapping and Applications to data from the Upper-Atmosphere Research Satellite, J. Geophys. Res., 100, 16491–16505, doi:10.1029/95JD01072, 1995.

Nash, E. R., Newman, P. A., Rosenfield, J. E., and Schoeberl, M. R.: An objective determination of the polar vortex using Ertel's potential vorticity, J. Geophys. Res., 101, 9471–9478, 1996.

Orsolini, Y. J., Urban, J., Murtagh, D. P., Lossow, S., and Limpasuvan, V.: Descent from the polar mesosphere and anomalously high stratopause observed in 8 years of water vapor and temperature satellite observations by the Odin Sub-Millimeter Radiometer, J. Geophys. Res., 115, 1–10, doi:10.1029/2009JD013501, 2010.

Pierce, R. B., Grose, W. L., and Russell, J. M.: Evolution of southern hemisphere air masses observed by HALOE, Geophys. Res. Lett., 21, 213–216, 1994.

Rodgers, C. D.: Inverse Methods for Atmospheric Soundings, World Scientific Publishing Co Pte. Ltd, 2000.

Scherhag, R.: Die explosionsartigen Stratosphärenerwärmungen des Spätwinters, 1951–52, Ber. Deut. Wetterdienst, 38, 51–63, 1952.

Schoeberl, M. R.: Stratospheric warmings: Observations and theory, Rev. Geophys., 16, 521–538, 1978.

Schoeberl, M. R., Lait, L. R., Newman, P. A., and Rosenfield, J. E.: The structure of the polar vortex, J. Geophys. Res., 97, 7859–7882, 1992.

Siskind, D. E., Eckermann, S. D., Lawrence, C., McCormack, J. P., and Randall, C. E.: On recent interannual variability of the Arctic winter mesosphere: Implications for tracer descent, Geophys. Res. Lett., 34, L09806, doi:10.1029/2007GL029293, 2007.

Sparling, L. C.: Statistical perspectives on stratospheric transport, Rev. of Geophys., 38, 417–436, 2000.

Straub, C., Murk, A., and Kämpfer, N.: MIAWARA-C, a new ground based water vapor radiometer for measurement campaigns, Atmos. Meas. Tech., 3, 1271–1285, doi:10.5194/amt-3-1271-2010, 2010.

Straub, C., Tschanz, B., Hocke, K., Kämpfer, N., and Smith, A. K.: Transport of mesospheric H_2O during and after the stratospheric sudden warming of January 2010: observation and simulation, Atmos. Chem. Phys., 12, 5413–5427, doi:10.5194/acp-12-5413-2012, 2012.

Sutton, R. T., Maclean, H., Swinbank, R., O'Neill, A., and Taylor, F. W.: High-Resolution Stratospheric Tracer Fields Estimated from Satellite Observations Using Lagrangian Trajectory Calculations, J. Atmos. Sci., 51, 2995–3005, 1994.

Waters, J. W., Froidevaux, L., Harwood, R. S., Jarnot, R. F., Pickett, H. M., Read, W. G., Siegel, P. H., Cofield, R. E., Filipiak, M. J., Flower, D. A., Holden, J. R., Lau, G. K. K., Livesey, N. J., Manney, G. L., Pumphrey, H. C., Santee, M. L., Wu, D. L., Cuddy, D. T., Lay, R. R., Loo, M. S., Perun, V. S., Schwartz, M. J., Stek, P. C., Thurstans, R. P., Boyles, M. A., Chandra, K. M., Chavez, M. C., Chen, G. S., Chudasama, B. V., Dodge, R., Fuller, R. A., Girard, M. A., Jiang, J. H., Jiang, Y. B., Knosp, B. W., LaBelle, R. C., Lam, J. C., Lee, K. A., Miller, D., Oswald, J. E., Patel, N. C., Pukala, D. M., Quintero, O., Scaff, D. M., Van Snyder, W., Tope, M. C., Wagner, P. A., and Walch, M. J.: The Earth Observing System Microwave Limb Sounder (EOS MLS) on the Aura satellite, IEEE T. Geosci. Remote., 44, 1075–1092, doi:10.1109/TGRS.2006.873771, 2006.

Wernli, H. and Davies, H.: A Lagrangian-based analysis of extratropical cyclones. I: The method and some applications, Q. J. Roy. Meteorol. Soc., 123, 467–489, 1997.

WMO: Scientific Assessment of Ozone Depletion, 2003.